A Generalized Correlation Coefficient: Application to DTI and Multi-Fiber DTI

Maxime Taquet[1,2], Benoît Macq[1], Simon K. Warfield[2]
[1] ICTEAM Institute, Université catholique de Louvain, Louvain-La-Neuve, Belgium
[2] Computational Radiology Laboratory, Harvard Medical School, Boston, USA
maxime.taquet@uclouvain.be

Abstract

Multi-fiber models have been introduced as an efficient and interpretable way of representing the diffusion signal in areas with crossing fibers. However, no metric has been provided to use multi-fiber features in registration. The normalized correlation coefficient is commonly used in registration of scalar images due to its invariance under linear transformations of the intensities. In this paper, we generalize the normalized correlation coefficient for tensor and multi-tensor images. The generalized invariance allows linear transformations of the diffusion eigenvalues in the logarithmic domain. We subsequently use it as a metric for block matching and show that multi-tensor features leverage the accuracy of the matching in areas with crossing fibers.

1. Introduction

Diffusion tensor imaging (DTI) provides an insight into the local diffusion of water molecules in tissues. Brain DTI enables the visualization and the characterization of fiber tracts in the white matter [5]. The development of registration methods for DTI has been motivated by the impossibility, in T1-weighted images, to distinguish structures in the white matter. Methods based on scalar features (*e.g.* [4, 7, 11]) and on the entire tensor information (*e.g.* [8, 14, 12]) have been proposed and it has been shown that methods based on the full tensor are better at detecting white matter differences [13].

A classical limitation of DTI is its incapacity to represent complex structures such as crossing fibers [6]. To overcome this limitation, novel sampling schemes (such as high angular resolution diffusion imaging, HARDI [10]) and novel model-based and model-free methods to analyze the diffusion weighted signals have emerged. These methods include Q-ball imaging (QBI), diffusion spectrum imaging (DSI), spherical deconvolution (SD) and generalized diffusion tensor imaging (GDTI), among others. Most of these methods aim at describing the general shape of the diffusion profile. Registration methods taking advantage of the information contained in these higher order diffusion models have been proposed [3, 2].

The principal drawback of these recent models is that they do not consider each fiber independently, and their interpretability is somewhat challenging. In contrast, multi-

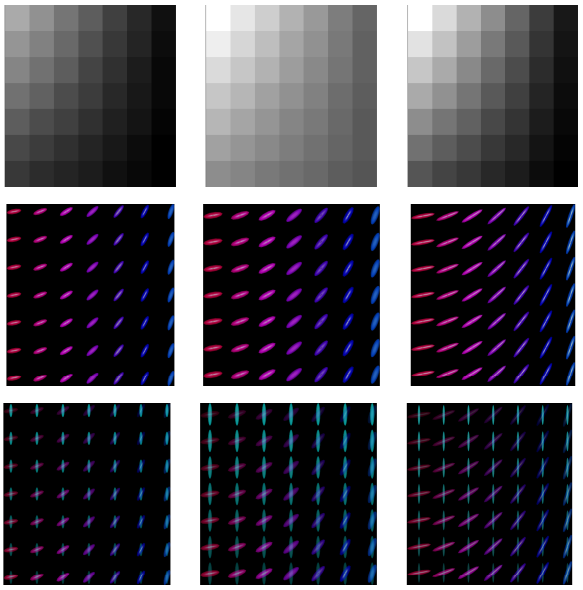

Figure 1. Just as the common normalized correlation coefficient is invariant under linear transformation of the image intensity, the generalized correlation coefficient is invariant under linear transformations of the diffusion eigenvalues in the log-domain. The three blocks of each row have a generalized correlation coefficient equal to 1 between each other. The color coding of the tensor images indicate the direction of the principal eigenvector, showing that linear transformations in the space of tensors and multi-tensors preserve the eigenvectors but affect the eigenvalues.

This investigation was supported in part by NIH grants R01 RR021885, R01 EB008015, R03 EB008680 and R01 LM010033. MT also thanks the F.R.S-FNRS and the B.A.E.F. for their financial support.

fiber models [10] represent the diffusion as a gaussian mixture model (GMM) in which each component corresponds to each fiber present at that location. Since the probability of the crossing of more than two fibers is extremely low, a second or third (one component being the isotropic diffusion) order GMM is typically used:

$$S = S_0 \left(f_0 e^{-b\boldsymbol{D}_{\text{iso}}} + f_1 e^{-b\boldsymbol{g}^T \boldsymbol{D}_1 \boldsymbol{g}} + f_2 e^{-b\boldsymbol{g}^T \boldsymbol{D}_2 \boldsymbol{g}} \right), \quad (1)$$

where D_{iso} is the diffusivity of free water, $\boldsymbol{D}_i$ are the anisotropic diffusion tensors and f_i are the relative volumetric occupancy. In this model, the water molecules are assumed to be in one of the channels with a probability corresponding to the volumetric occupancy of that channel in the voxel. With such a model, the diffusion parameters can be computed independently for each fiber bundle. This property is of central interest for tractography and fiber integrity assessment [9]. Besides, considering fiber bundles independently should allow the definition of novel metric for matching multi-tensor diffusion images, with the expectation to further improve the characterization of white matter differences between subjects. However, to the best of our knowledge, no such metric has been defined and it is precisely the goal of this paper to initiate this investigation.

The value of white matter diffusivity varies from one subject to the other, partly explained by the difference in myelination between individuals. The metric used for registration of diffusion images shall therefore account for this variability. In this paper, we generalize the normalized correlation coefficient, widely used in block matching of scalar images for its invariance under linear transformations of the intensities in the image block. In particular, our generalized correlation coefficient is invariant under linear transformations of the logarithm of the eigenvalues of the diffusion tensors, while being sensitive to changes in orientation of these tensors (Fig. 1).

The remaining of this paper is organized as follows. Section 2 introduces the generalized correlation coefficient and specifies a particular expression for single-tensor and multi-tensors DTI. Section 3 shows prior results on a brain diffusion image. A comparison between single-tensor and multi-tensor matching in terms of accuracy and robustness is provided. Section 4 summarizes the paper.

2. Methods

The normalized correlation coefficient used for block matching in scalar images is generalized in this section to single-tensor and multi-tensor images. We proceed in two steps. First, we extend the normalized correlation coefficient to its most general form and determine the constraints on its components to maintain its invariance property and its interpretability as a similarity metric. Second, we make sound choices of these components for the single-tensor and multi-tensor cases.

2.1. Generalized correlation coefficient

Let R and S be two image blocks with N voxels whose locations are referred to as $\boldsymbol{x}$. The common definition for the normalized correlation coefficient between R and S is:

$$\rho(R,S) = \left\langle \frac{R-\mu_R}{||R-\mu_R||}, \frac{S-\mu_S}{||S-\mu_R||} \right\rangle,$$

where μ_R is the mean of R over the image domain. This coefficient is invariant under any linear transformation of the image values:

$$R' = aR + b \Rightarrow \rho(R',S) = \rho(R,S). \quad (2)$$

Ruiz-Alzola *et al*. [8] proposed to extend the normalized correlation coefficient to cope with vector images[1]. Their idea relies on rewriting $R - \mu_R$ as

$$R - \mu_R = R - \langle R, T \rangle \frac{T}{||T||^2},$$

where they define T as an image of the same modality as R (scalar, vector or tensor) containing only 1's. The invariance property becomes:

$$R' = aR + bT \Rightarrow \rho(R',S) = \rho(R,S). \quad (3)$$

In the remaining of this section, we keep T as a general constant image and address the following question: can the normalized correlation coefficient be further generalized by allowing the inner product $\langle .,. \rangle$ to be a more general scalar mapping (*i.e*. a mapping from a pair of image blocks to the scalar field)? We denote by $m(X,Y)$ this scalar mapping and define the generalized norm as $n_m^2(X) = m(X,X)$.

In its most general form, the generalized correlation coefficient therefore reads:

$$\rho(R,S) = m\left(\frac{R - m(R,T)T}{n_m(R - m(R,T)T)}, \frac{S - m(S,T)T}{n_m(S - m(S,T)T)} \right),$$

where $m(R,T)T$ can be thought of as a generalization of the mean image (the projection of the image on the constant image) and the denominators can be thought of as a generalization of the variance images. In the next section, the properties required by m to ensure invariance and interpretability of the correlation coefficient are exposed.

2.2. Valid Scalar Mappings

Not all scalar mappings preserve the invariance property (3) and the interpretability of the resulting correlation coefficient as a similarity metric. We call *valid mappings*

[1] They also present a tensor extension by rasterizing the tensor to a vector which, however, does not account for the structure of the tensor space.

the scalar mappings that preserve the invariance and interpretability of the correlation coefficient. In the following, we derive the conditions on m to be a valid mapping.

Let us start by deriving the conditions on m for the correlation coefficient to be interpretable. As a similarity measure, we want the correlation coefficient to be equal to 1 when the two image blocks are identical:

$$\rho(R, R) = 1, \tag{4}$$

and we want it to be lower or equal to 1 in absolute value in any other case:

$$|\rho(R, S)| \leq 1. \tag{5}$$

Condition (4) is satisfied if

$$m(aR, aR) = a^2 m(R, R), \tag{6}$$

and condition (5) is satisfied if

$$|m(R, S)| \leq n_m(R) n_m(S). \tag{7}$$

We also want the correlation coefficient to be symmetric, which is satisfied if the mapping is symmetric:

$$m(R, S) = m(S, R). \tag{8}$$

Now, the invariance under linear transformations, *i.e.*

$$\rho(aR + bT, S) = \rho(R, S),$$

is preserved if the following two conditions are respected:

$$\begin{aligned} m(aR, T) &= a\, m(R, T) && (9)\\ m(R + T, T) &= m(R, T) + m(T, T). && (10) \end{aligned}$$

Note that these two last conditions are related to cases where one of the argument of the mapping is the constant image T. Linearity of the mapping with respect to any pair of images is a sufficient but not a necessary condition for valid mappings. Therefore, the set of valid scalar mappings includes, but is not restricted to, inner products. This property will turn out to be highly relevant when defining a generalized correlation coefficient in the multi-tensor case.

2.3. The Single-Tensor Case

The space of symmetric positive semi-definite matrices is not a vector space in the canonical parameterization. However, Arsigny *et al.* [1] proposed a vector space structure for diffusion tensor processing by representing every diffusion matrix by its matrix logarithm. An inner product can then be defined in the log-domain. Given two tensor image blocks R and S defined on a domain Ω such that for $\boldsymbol{x} \in \Omega$, R takes the value $R(\boldsymbol{x})$, the inner product can be defined as:

$$\begin{aligned} m_1(R, S) &= \sum_{\boldsymbol{x} \in \Omega} \langle \log R(\boldsymbol{x}), \log S(\boldsymbol{x}) \rangle && (11)\\ &= \sum_{\boldsymbol{x} \in \Omega} \text{Trace}\left(\log R(\boldsymbol{x})^T \log S(\boldsymbol{x}) \right). && (12) \end{aligned}$$

To satisfy conditions (6-10), the basic arithmetic operations need also be defined in the log-domain so that the invariance property of the correlation coefficient becomes:

$$\begin{aligned} \log R'(\boldsymbol{x}) &= a \log R(\boldsymbol{x}) + bT(\boldsymbol{x}) && (13)\\ \Rightarrow \rho(R', S) &= \rho(R, S). && (14) \end{aligned}$$

Since no constraint is imposed on T, its choice is driven by the targeted invariance. By choosing T as a tensor image whose voxels are proportional to the identity matrix, *i.e.*:

$$T(\boldsymbol{x}) = T_0 \propto \mathrm{I}_3, \ \forall \boldsymbol{x} \in \Omega,$$

the invariance (14) becomes:

$$R'(\boldsymbol{x}) = e^b R^a \Rightarrow \rho(R', S) = \rho(R, S).$$

This invariance preserves the eigenvectors and allows linear transformations of the eigenvalues $\lambda_1, \lambda_2, \lambda_3$ in the log-domain:

$$\lambda_i' = e^b \lambda_i^a. \tag{15}$$

Any pair of blocks having their eigenvectors aligned at each voxel, with eigenvalues related by (15) will thus be considered a perfect match and have a correlation coefficient equal to 1.

2.4. The Multi-Tensor Case

In the multi-tensor model, the diffusion signal is assumed to emanate from a gaussian mixture model as in (1). Since the fractions f_i sum up to 1, the multi-tensor images can be parameterized by:

$$R(\boldsymbol{x}) = \big(f_1(\boldsymbol{x}), R_1(\boldsymbol{x}), f_2(\boldsymbol{x}), R_2(\boldsymbol{x})\big).$$

The expression of the signal (1) tells us that the points $R_{12} = (f_1, R_1, f_2, R_2)$ and $R_{21} = (f_2, R_2, f_1, R_1)$ need to be identified. This folding of the space makes it hard, if not impossible, to represent it as a vector space. Consequently, an inner product for mutli-tensor images cannot be defined and a more general scalar mapping m is required.

Fiber-crossings only occur sparsely in the image. We therefore want our generalized correlation coefficient to tend towards the single-tensor inner product when only one fiber is present in all voxels of both image blocks. In other words, we want:

$$\lim_{\substack{f_1 \to 1, f_2 \to 0 \\ g_1 \to 1, g_2 \to 0}} m(R, S) = m_1(R_1, S_1), \tag{16}$$

where $R = (f_1, R_1, f_2, R_2)$ and $S = (g_1, S_1, g_2, S_2)$. This condition is added to conditions (6-10) of valid scalar mappings.

We start by separating the spatial dependency in the scalar mapping, just as in (12):

$$m(R, S) = \sum_{\boldsymbol{x} \in \Omega} m_l(R(\boldsymbol{x}), S(\boldsymbol{x})), \tag{17}$$

where m_l is now a scalar mapping in the space of multi-tensors (and not multi-tensor images). A natural generalization of (12) would come from defining m_l as a linear combination of single-tensor inner products, with coefficients proportional to the fractions. In this way, when the fractions tend to zero, the corresponding terms in the linear combination vanish and the scalar mapping sums up to a single-tensor inner product.

Pairing the tensors of the multi-tensor model in two clusters on which single-tensor inner products are computed requires caution. Indeed, there is no sound reason to pair $R_1(\boldsymbol{x})$ with $S_1(\boldsymbol{x})$ rather than $S_2(\boldsymbol{x})$. We will select, at each voxel, the pairings that maximizes the absolute value of the scalar mapping. Let d_1 and d_2 be the two possible linear combinations:

$$d_1 = f_1 g_1 \langle R_1, S_1 \rangle + f_2 g_2 \langle R_2, S_2 \rangle \quad (18)$$
$$d_2 = f_1 g_2 \langle R_1, S_2 \rangle + f_2 g_1 \langle R_2, S_1 \rangle . \quad (19)$$

The local scalar mapping is defined as:

$$m_l(R, S) = \arg\max_{d_i} |d_i|. \quad (20)$$

The absolute value is required to satisfy (16): in the limit of the single-tensor case, d_1 or d_2 would tend to zero while the other one, equal to single-tensor scalar product, might be negative.

To verify the invariance property of the resulting correlation coefficient, both the constant element T and the basic arithmetics (multiplication by a scalar and addition of the constant element) need to be defined for multi-tensor images. The constant element naturally comes as:

$$T(\boldsymbol{x}) \propto (0.5, T_0, 0.5, T_0), \quad \forall \boldsymbol{x} \in \Omega.$$

As for the arithmetic operations, they are again defined in the log-domain. The multiplication by a scalar is naturally generalized by:

$$a(f_1, \log R_1, f_2, \log R_2) = (f_1, a \log R_1, f_2, a \log R_2). \quad (21)$$

The addition of the constant element to a multi-tensor image can be defined as:

$$R + T = (f_1, \log(R_1) + T_0, f_2, \log(R_2) + T_0). \quad (22)$$

Note that only the addition of the constant element is required to define the generalized correlation coefficient.

It is straightforward to check that these definitions of scalar mapping and basic operations respect conditions (6-10). The invariance property can now be expanded:

$$\begin{aligned} R' = \; & aR + bT \; = (f_1, e^b R_1^a, f_2, e^b R_2^a) \\ \Rightarrow \; & \rho(R', S) \; = \rho(R, S) \end{aligned} \quad (23)$$

This invariance is a natural generalization of the invariance property for single-tensor images. In terms of eigenvalues, (23) reads:

$$\begin{aligned} & \lambda_i' = e^b \lambda_i^a \text{ and } \kappa_i' = e^b \kappa_i^a \\ \Rightarrow \; & \rho(R', S) = \rho(R, S), \end{aligned} \quad (24)$$

where λ_i are the eigenvalues of R_1 and κ_i are the eigenvalues of R_2.

Any pair of blocks having their eigenvectors aligned at each voxel in both channels, with equal fractions and with eigenvalues related by (15) will thus be considered a perfect match and have a correlation coefficient equal to 1. On the contrary, if the eigenvectors are misaligned, the correlation coefficient will not be preserved.

3. Experiments and Results

We assess the ability of the metric to distinguish between anatomical features under the influence of deformation and noise. Diffusion weighted (DW) signals were obtained for a full brain volume and both a single-tensor DTI and a multi-tensor DTI models were constructed using the technique described in [9]. Throughout the volume, 400 anatomical landmarks presenting fiber crossings were detected (Fig. 2(a)). A random smooth synthetic field was applied to both the single-tensor and the multi-tensor DTI (Fig. 2(b)).

Block matching with the generalized correlation coefficient was used to estimate the location of the anatomical features in the deformed image. The blocks were 7×7 and correspondences were sought in regions of size 31×31. Only one iteration at one scale was performed. Symmetric matrices of gaussian noise were then applied in the log-domain at each voxel in the single-tensor DTI and in the multi-tensor DTI (independently in each channel). The standard deviation of the noise goes from 0% to 20% of the mean Frobenius norm of the log-tensor computed in the single-tensor DTI. Two quantities were measured: the accu-

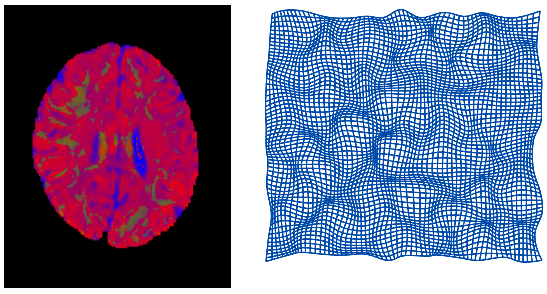

(a) (b)

Figure 2. (a) Repartition of the volumetric fractions encoded as a RGB map. Green areas indicate the presence of a second fiber. (b) Synthetic random smooth deformation field applied to the images.

racy and the saliency of the correspondence. The accuracy is assessed by the target registration error (Fig. 3 and 4(a)). The multi-tensor features appear to be more robust to noise. For an additive gaussian noise of 10% and over, the difference of accuracy is significant on average ($p < 10^{-9}$). The saliency of the correspondence is computed as the difference between the correlation coefficient of the correct correspondence and the mean of the correlation coefficient in the search region, expressed as a number of standard deviations (Fig. 3 and 4(b)). The saliency of the correct match is significantly stronger on average using multi-tensor features than for single-tensor features ($p < 10^{-15}$). This tells us that, although the correct match may no more be the local maximum of the similarity map in presence of noise, its similarity value is still much larger than the average metric value in the region of interest. Qualitative results are also depicted in Fig. 5 where multi-tensors appear at the interface between the white matter and the grey matter.

The volumetric fractions f_i depend on the angle at which two fibers cross each other. This phenomenon, known as the partial volume effect, modifies the diffusion signal at every voxel of fiber crossing areas. Therefore, the content of both the multi-fiber and the single-tensor models will be modified. The extreme case occurs when two fibers are crossing in one image but lie in separate voxels in the other images. This phenomenon was simulated by setting to zero the smallest fraction at each voxel in the deformed multi-tensor image. We then compared the results by performing (1) single-tensor registration between the resulting single tensor image and the single-tensor model of the original image and (2) multi-tensor registration between the resulting single-tensor image and the original multi-tensor model.

The results in terms of accuracy and saliency for the same 400 anatomical landmarks are reported on Fig. 4(c-d). The differences between the two features are highly significant ($p < 10^{-15}$), although not surprising. Indeed, the multi-tensor model will still contain part of the information used for the matching, while the single-tensor model will present a very different content.

Since the generalized correlation coefficient for multi-tensor images is equal to the single-tensor one in regions with single fibers, the better alignment of multi-tensor models in crossing fiber areas is obtained at no cost for the single-fiber areas.

4. Conclusion

In this paper, the normalized correlation coefficient has been generalized to tensor and multi-tensor images. The generalized invariance allows linear transformations of the tensor eigenvalues in the log-domain. Its use in block matching shows overall good performances and significantly better performances when used with multi-tensor images, leveraging the registration accuracy in areas with fiber crossing. In a future work, a comparison with existing registration of high order diffusion models should be performed.

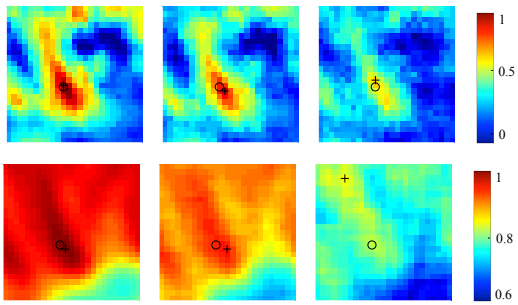

Figure 3. The use of multi-tensor features allow more accurate and more robust matchings. This figure depicts the similarity maps in the presence of 0% (left), 10% (middle) and 20% (right) additive gaussian noise, for both multi-tensor block matching (top) and single-tensor block matching (bottom). The ∘ indicates the correct match and the + indicates the maximum of the similarity metric.

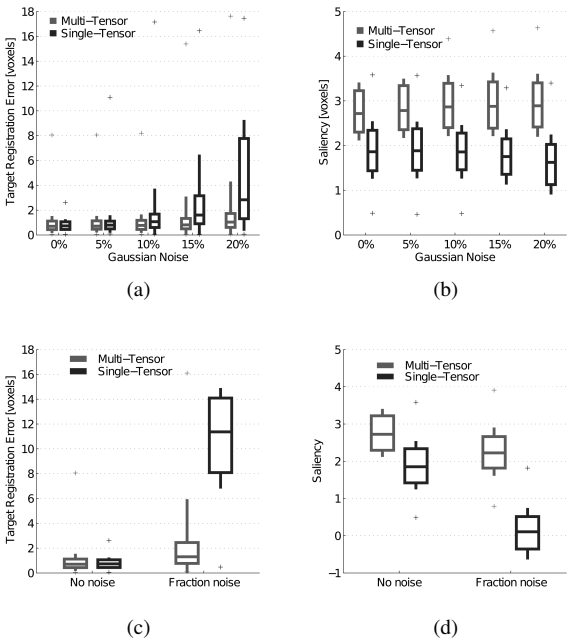

Figure 4. Saliency and accuracy compared for both multi-tensor and single-tensor block matching, (a-b) in the presence of additive gaussian noise, (c-d) in the case where one of the crossing fiber disappears from the block, *e.g.* due to a different crossing angle.

References

[1] V. Arsigny, P. Fillard, X. Pennec, and N. Ayache. Fast and simple calculus on tensors in the log-euclidean framework. *MICCAI 2005*, pages 115–122, 2005.

[2] A. Barmpoutis and B. Vemuri. Groupwise registration and atlas construction of 4th-order tensor fields using the r+ riemannian metric. *MICCAI 2009*, pages 640–647, 2009.

[3] A. Barmpoutis, B. Vemuri, and J. Forder. Registration of

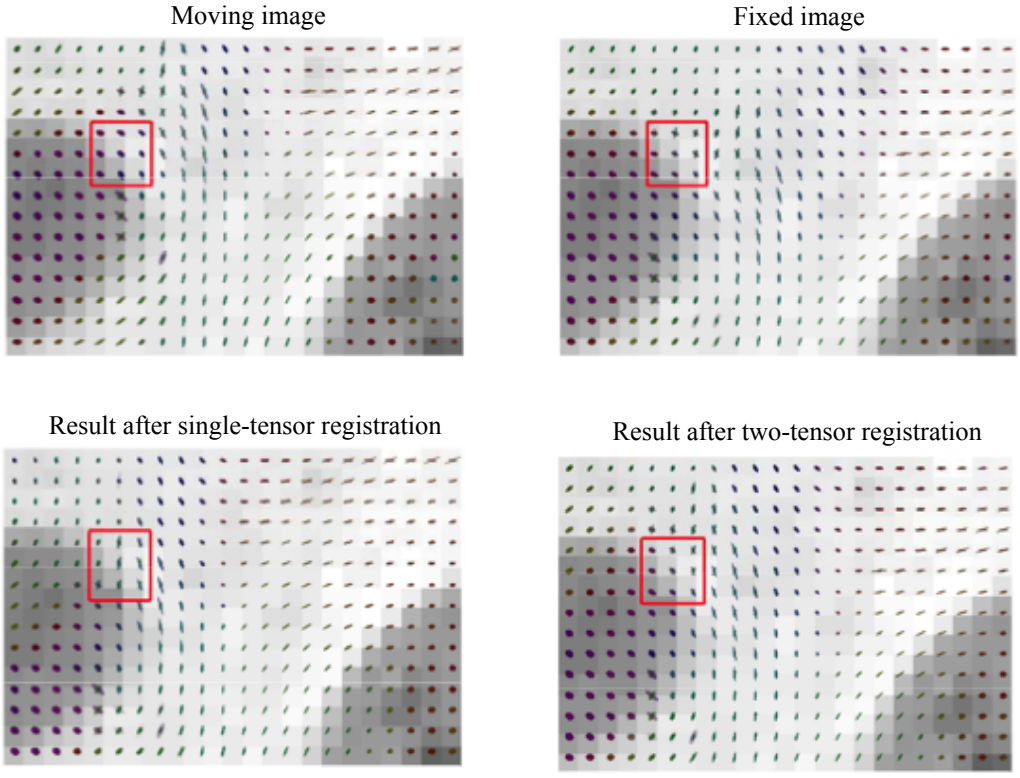

Figure 5. Results of the registration using block matching and the generalized correlation coefficient for single-tensor and multi-tensor under 10% of gaussian noise. Multi-tensor registration achieves better results in areas with multiple fibers such as within the boxes.

high angular resolution diffusion mri images using 4-th order tensors. *MICCAI 2007*, pages 908–915, 2007.

[4] A. Guimond, C. Guttmann, S. Warfield, and C. Westin. Deformable registration of dt-mri data based on transformation invariant tensor characteristics. In *IEEE ISBI 2002*, pages 761–764, 2002.

[5] M. Moseley, Y. Cohen, J. Kucharczyk, J. Mintorovitch, H. Asgari, M. Wendland, J. Tsuruda, and D. Norman. Diffusion-weighted mr imaging of anisotropic water diffusion in cat central nervous system. *Radiology*, 1990.

[6] E. Ozarslan and T. Mareci. Generalized diffusion tensor imaging and analytical relationships between diffusion tensor imaging and high angular resolution diffusion imaging. *Magnetic Resonance in Medicine*, 50(5):955–965, 2003.

[7] H. Park, M. Kubicki, M. Shenton, A. Guimond, R. McCarley, S. Maier, R. Kikinis, F. Jolesz, and C. Westin. Spatial normalization of diffusion tensor mri using multiple channels. *Neuroimage*, 20(4):1995–2009, 2003.

[8] J. Ruiz-Alzola, C. Westin, S. Warfield, C. Alberola, S. Maier, and R. Kikinis. Nonrigid registration of 3d tensor medical data. *Medical Image Analysis*, 6(2):143–161, 2002.

[9] B. Scherrer and S. Warfield. Toward an accurate multi-fiber assessment strategy for clinical practice. In *IEEE ISBI 2011*, pages 2140–2143, 2011.

[10] D. Tuch, T. Reese, M. Wiegell, N. Makris, J. Belliveau, and V. Wedeen. High angular resolution diffusion imaging reveals intravoxel white matter fiber heterogeneity. *Magnetic Resonance in Medicine*, 48(4):577–582, 2002.

[11] J. Yang, D. Shen, C. Davatzikos, and R. Verma. Diffusion tensor image registration using tensor geometry and orientation features. *MICCAI 2008*, pages 905–913, 2008.

[12] B. Yeo, T. Vercauteren, P. Fillard, J. Peyrat, X. Pennec, P. Golland, N. Ayache, and O. Clatz. Dt-refind: Diffusion tensor registration with exact finite-strain differential. *IEEE Trans. on Medical Imaging*, 28(12):1914–1928, 2009.

[13] H. Zhang, B. Avants, P. Yushkevich, J. Woo, S. Wang, L. McCluskey, L. Elman, E. Melhem, and J. Gee. High-dimensional spatial normalization of diffusion tensor images improves the detection of white matter differences: an example study using amyotrophic lateral sclerosis. *Medical Imaging, IEEE Transactions on*, 26(11):1585–1597, 2007.

[14] H. Zhang, P. Yushkevich, D. Alexander, and J. Gee. Deformable registration of diffusion tensor mr images with explicit orientation optimization. *Medical Image Analysis*, 10(5):764–785, 2006.